Monthly Notices
of the
ROYAL ASTRONOMICAL SOCIETY

MNRAS **495,** 510–524 (2020)
Advance Access publication 2020 April 29

doi:10.1093/mnras/staa1188

The excitation temperature of the CH 3335-MHz line

Erin M. Dailey,[1]★ Allison J. Smith,[1] Loris Magnani,[1] B.-G. Andersson[2] and William T. Reach[2]

[1]*Department of Physics and Astronomy, University of Georgia, Athens, GA 30602, USA*
[2]*Stratospheric Observatory for Infrared Astronomy, Universities Space Research Association, NASA Ames Research Center, MS 232-11, Moffett Field, CA 94035, USA*

Accepted 2020 April 24. Received 2020 April 23; in original form 2019 December 17

ABSTRACT

Molecular hydrogen is the main constituent of dense molecular clouds, but is expected to also be a dominant constituent in many environments where CO can no longer be seen, the so-called 'CO-dark molecular gas'. Based on comparisons of ultraviolet spectroscopy of H_2 and optical line observations (4300 Å), CH is a prime candidate to trace H_2. Since the optical line (and the UV lines at 3143, 3890, and 3878 Å) require bright background sources (and the CH $N = 2 \leftarrow 1$ ground state rotation line at 149 μm requires space-based, or stratospheric, observations), the hyperfine structure transition at 3335 MHz is a potentially important tool for probing the CO-dark molecular gas. However, the excitation of this transition is complicated, and has often been found to be inverted, making column density determinations uncertain. To clarify the potential use of the 3.3-GHz line as a proxy for H_2, we have observed the CH 3335-MHz line with the Arecibo 305-m radio telescope along 16 lines of sight towards stars with existing measurements of the 4300-Å line. By comparing the CH column densities from optical and UV absorption lines to the CH radio emission line, we can derive the excitation temperature (T_{ex}) of the 3335-MHz transition. We obtain a wide range of excitation temperatures for nine lines of sight, including some with $|T_{ex}| < 5$ K. The common assumption that T_{ex} for the 3335-MHz line is always much larger than the background temperature (T_{bg}) is not always warranted and can lead to significant errors in the value of N(CH).

Key words: ISM: clouds – ISM: lines and bands – ISM: molecules.

1 INTRODUCTION

The most commonly used tracer of molecular hydrogen in the interstellar medium (ISM) is the J = 1–0 transition of CO at 115 GHz. It has long been clear from both observations (e.g. Federman et al. 1980) and theory (Federman, Glassgold & Kwan 1979; van Dishoeck & Black 1986, 1988) that H_2 is, because of significant self-shielding in the Lyman and Werner bands, less prone to photodissociation than CO and hence will survive to smaller column densities. Until recently, the assumption was made that the transition region between molecular gas with N(CO) too low for detection at 115 GHz and that with detectable CO(1–0) emission was relatively thin and contained little mass (e.g. Andersson & Wannier 1993), or consisted of a minor population of diffuse molecular clouds (e.g. Lada & Blitz 1988; van Dishoeck & Black 1989).

With the lack of detectable CO emission, other species were proposed as tracers of this transitional gas, including OH (Wannier et al. 1993; Barriault et al. 2010; Allen et al. 2012; Cotten et al. 2012; Allen, Hogg & Engelke 2015; Xu et al. 2016; Tang et al. 2017; Li et al. 2018) and CH (Sandell, Stevens & Heiles 1987; Magnani & Onello 1993; Xu & Li 2016). In particular, the latter has been found to be a reliable tracer of H_2 over several orders of magnitude of $N(H_2)$ using the optical 4300-Å line (e.g. Sheffer & Federman 2007), the 3335 MHz hyperfine, Λ-doubled, F = 1–1 transition (Mattila 1986), and recently through the $N = 2 \leftarrow 1$ ground state rotation line at 149 μm (Wiesemeyer et al. 2018).

The possible existence of substantial molecular gas in the ISM that is not spectroscopically detectable via the CO(1–0) emission line was discussed by Grenier, Casandjian & Terrier (2005). By using a combination of colour-corrected dust maps, gamma-ray data from EGRET, and N(H I) and CO(1–0) emission maps, they identified regions with substantial gas column density not traced by the H I or CO data. At mid to high latitudes, these regions appear to form extensive haloes surrounding local molecular clouds (cf. Andersson & Wannier 1993) and are believed to represent a molecular component currently referred to as 'CO-dark molecular gas' (for brevity, we will refer to this gas as CO-dark gas, acknowledging that fully atomic or ionized gas is, of course, by definition, also 'CO-dark'). Based on estimates in Grenier et al. (2005) CO-dark gas was thought, on galactic scales, to contribute

★ E-mail: dailey7@uga.edu

about an equal molecular mass to that detected through CO(1–0) emission. However, subsequent studies have substantially decreased the estimated CO-dark gas balance (e.g. Donate & Magnani 2017).

The CH molecule was one of the first found in the ISM (Dunham & Adams 1937a, b) via the 4300-Å line in the *A*–*X* band. Studies of this line towards background early-type stars reveal that there is a good correlation between N(CH) and $N(H_2)$ (e.g. Federman 1982; Danks, Federman & Lambert 1984; Sheffer et al. 2008). In addition to the 4300-Å line, the *B*–*X* band offers the 3886- and 3890-Å lines as agents for determining robust values for N(CH) (e.g. Chaffee 1974, 1975; Weselak et al. 2008). Studies of this type were used by Mattila (1986) to establish the low extinction ($A_V \lesssim 3$ mag) end of his empirical relation between N(CH) and $N(H_2)$. For low extinctions, the $N(CH)/N(H_2)$ ratio is very robust at $4.3 \pm 1.9 \times 10^{-8}$ (Liszt & Lucas 2002), and thus N(CH) can lead to reliable estimates of $N(H_2)$.

In addition to optical and UV observations of interstellar absorption lines towards early-type stars, a recent paper by Wiesemeyer et al. (2018) proposes that the $N = 2 \leftarrow 1$ ground state transition of CH at 149 μm can also be used to obtain N(CH) and, consequently, $N(H_2)$. The absorption line connects the N = 1, J = 1/2 ground state to the N = 2, J = 3/2 states comprised of two triplets of hyperfine structure lines. The lines are thin and unsaturated and arise in low-density molecular gas. However, while the Galaxy is more transparent at infrared than optical wavelengths, the atmosphere is not and observations of these lines require space/stratospheric observatories.

In the radio regime, the $^2\Pi_{1/2}$, J = 1/2, ground state, lambda doubled, hyperfine, F = 1–1 main line at 3335.479 MHz (Truppe et al. 2014) provides a reasonable alternative to CO or OH for tracing low-density molecular gas. The two other hyperfine components of this transition are 3263.793 MHz (F = 0–1) and 3349.193 MHz (F = 1–0) (Truppe et al. 2014). Under normal excitation conditions, these satellite lines are one-half the intensity of the main line.

N(CH) is obtained from the velocity-integrated antenna temperature of the 3335-MHz line [$W(\mathrm{CH}) \equiv (\eta_\mathrm{B})^{-1} \int T_\mathrm{A}\, \mathrm{d}v$ (mK km s^{-1})] using an equation from Liszt & Lucas (2002):

$$N(\mathrm{CH}) = 2.82 \times 10^{11} (\eta_\mathrm{f})^{-1} [T_\mathrm{ex}/(T_\mathrm{ex} - T_\mathrm{bg})]\, W(\mathrm{CH}), \quad (1)$$

where η_B is the beam efficiency of the telescope, η_f is the filling factor of molecular gas in the beam, T_ex is the excitation temperature, and T_bg is the background temperature. At 3.3 GHz, $T_\mathrm{bg} \approx 2.8$ K (e.g. Fixsen et al. 2011). If $|T_\mathrm{ex}| \gg T_\mathrm{bg}$, then N(CH) is directly proportional to W(CH). Early measurements showed that the 3335-MHz transition was inverted with T_ex ranging from −9 to −60 K (Rydbeck et al. 1976; Hjalmarson et al. 1977; Genzel et al. 1979). Specifically, Rydbeck et al. (1976) used on–off observations of Perseus and Orion Arm clouds towards Cassiopeia A to determine $T_\mathrm{ex} = -15 \pm 5$ K. Shortly thereafter, Lang & Willson (1978) used this value to determine N(CH) in a comparison of column densities from radio and optical observations. They found that the radio and optical column densities differed by less than a factor of two, with the ratio of $N_\mathrm{radio}/N_\mathrm{optical} = 1.68 \pm 0.34$ lending credence to the idea that the factor $T_\mathrm{ex}/(T_\mathrm{ex} - T_\mathrm{bg})$ could be considered to have a value near unity. Moreover, the resulting N(CH) values were linear with the colour excess for $E(B - V) < 0.6$ mag, for both the optical and radio observations. Genzel et al. (1979) used on–off observations similar to Rydbeck et al. (1976) and found $T_\mathrm{ex} = -60 \pm 30$ K for the 3335-MHz line from dust clouds 3C 123 and L1500. On the basis of these results, most radio astronomers derive N(CH) directly from W(CH) (3335) assuming $T_\mathrm{ex} = -15 \pm 5$ K, $T_\mathrm{ex} = -60 \pm 30$ K, or $|T_\mathrm{ex}| \gg T_\mathrm{bg}$.

In a key paper, Lien (1984) also compared radio and optical column densities of CH for a few lines of sight traversing diffuse or translucent gas. He found that T_ex from radio and optical observations were in the range of approximately 6–25 K with one line of sight where T_ex is approximately −4 K, while T_ex from optical and ultraviolet observations were approximately −1 or 1 K. Not surprisingly, the column densities of the observed lines of sight derived using T_ex in this range are often significantly different than under the assumption $|T_\mathrm{ex}| \gg T_\mathrm{bg}$. In addition to differing excitation temperatures, Lien (1984) attributed the reasons for the discrepancy in column density to several additional factors: In deriving $N(\mathrm{CH})_\mathrm{radio}$, both a filling factor, η_f, and T_ex have to be assumed. Moreover, $N(\mathrm{CH})_\mathrm{optical}$ measures the column density only to the star, whereas $N(\mathrm{CH})_\mathrm{radio}$ traces gas along the entire line of sight. If there is substantial CH beyond the target star for the absorption lines studies, then a direct comparison of the column densities between the two techniques would not be fruitful. Finally, the beam size of the radio observations is on the order of arc minutes compared with the nearly infinitesimal solid angle of the optical line of sight. Thus, variations in cloud structure on small scales can produce discrepancies in the column densities estimated from the two methods.

Lien (1984) also proposed that if the above issues aside from the value of T_ex could be resolved, then replacing $N(\mathrm{CH})_\mathrm{radio}$ with the more robust $N(\mathrm{CH})_\mathrm{optical}$ estimate would allow one to solve equation (1) directly for T_ex. In this paper, we calculate T_ex by this technique. We detected CH 9 cm emission for 9 of the 16 lines of sight in our sample for which optical and UV CH absorption lines are available. We then examine whether the conditions described above can permit us to determine T_ex for the given line of sight. The paper is organized as follows: Section 2 describes the radio observations we made to compare with the optical ones from the literature. The results are described in Section 3, and some of the problems encountered in deriving T_ex are discussed in Section 4. The individual lines of sight are discussed is Section 5, and the paper closes with a summary.

2 OBSERVATIONS

The CH observations for this project were made between 2017 August and December, using the Arecibo 305-m radio telescope. We used the upper *S*-band receiver that produced system temperatures of ∼30 K on the sky with a beam size at 3335 MHz of 1.3 arcmin × 1.5 arcmin elongated in azimuth. At Arecibo, we measured the beam efficiency by observing extragalactic continuum sources. Our observations were made before and after Hurricane Maria which struck the island of Puerto Rico on 2017 September 20. The damage done by the hurricane to the facilities at Arecibo significantly changed the beam efficiency. At 3335 MHz, η_B was 0.57 ± 0.02 before the hurricane and 0.40 ± 0.04 after.

The spectrometer was the Wideband Arecibo Pulsar Processor (WAPP) divided into eight boards configured to observe the CH lines at 3 GHz (9 cm) with a bandwidth of 1.5625 MHz for each section resulting in a velocity coverage of 141 km s^{-1} and a resolution of 0.07 km s^{-1} per channel (before smoothing) for the 3335-MHz line. The CH 3335-MHz line was in boards 1 and 2 (for redundancy), the 3349-MHz line was in boards 3 and 4, and the 3264-MHz line was in boards 5 and 6. Boards 7 and 8 were centred on 3139 and 3195 MHz, respectively, in an unsuccessful effort to detect H_2CS and CH_3CHO. Each final spectrum consisted of between 5 and 24 five-minute scans taken in ON-source mode only. A sixth order baseline was removed from the summed spectrum to produce the spectra shown in Fig. 1. Typical rms noise levels were between 9 and 22 mK for a velocity resolution of 0.069 km s^{-1}.

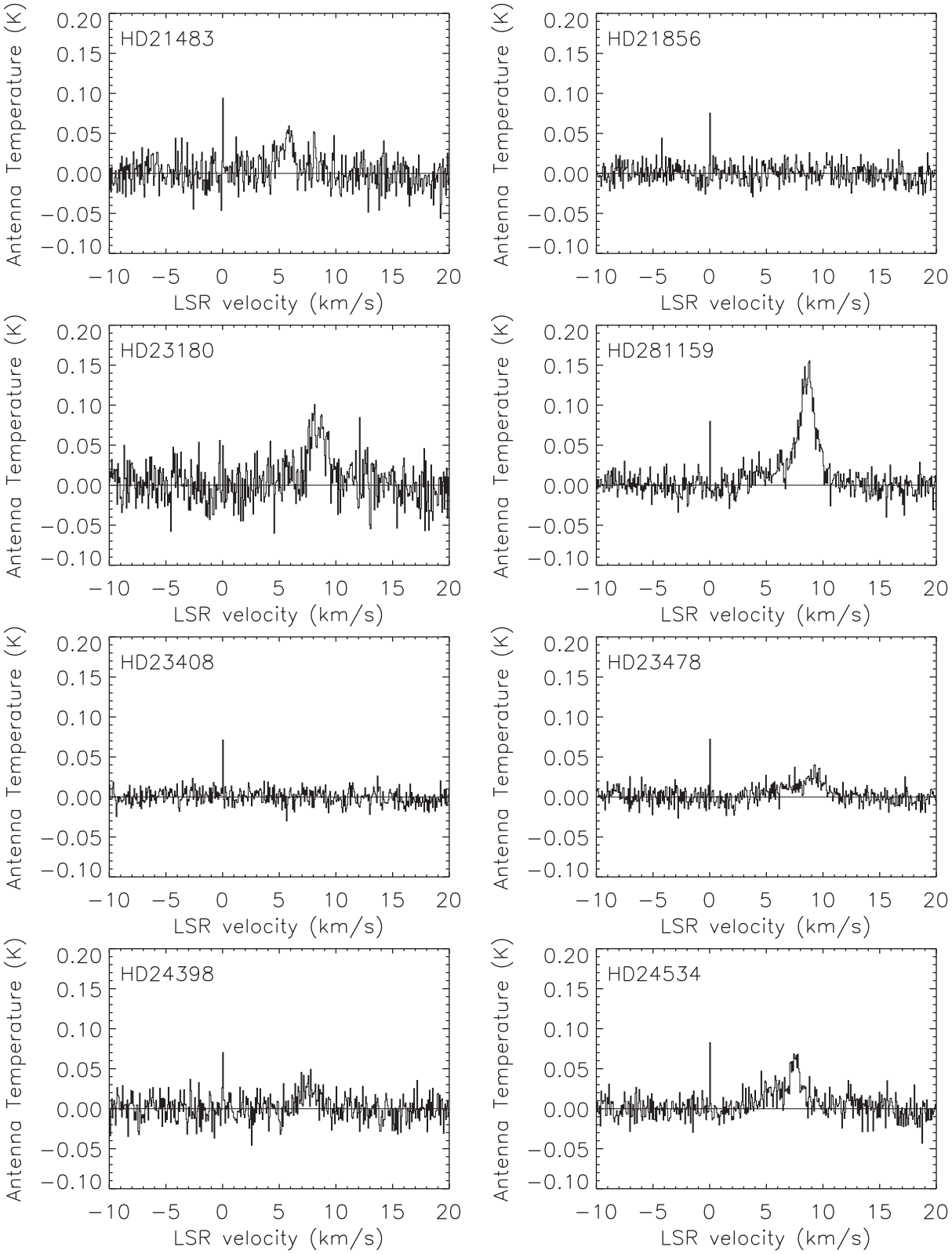

Figure 1(a). (a) CH 3335 MHz spectra for the first eight lines of sight in Table 1. The spike sometime visible at $v_{\rm LSR} = 0.0$ km s^{-1} is due to internal interference. (b) Same as (a) for the remaining eight lines of sight in Table 1. (c) CH 3349 MHz spectra for the first eight lines of sight in Table 1. The spike sometime visible at $v_{\rm LSR} = 0.0$ km s^{-1} is due to internal interference. (d) Same as (c) for the remaining eight lines of sight in Table 1. (e) CH 3264 MHz spectra for the first eight lines of sight in Table 1. The spike sometime visible at $v_{\rm LSR} = 0.0$ km s^{-1} is due to internal interference. (f) Same as (e) for the remaining eight lines of sight in Table 1.

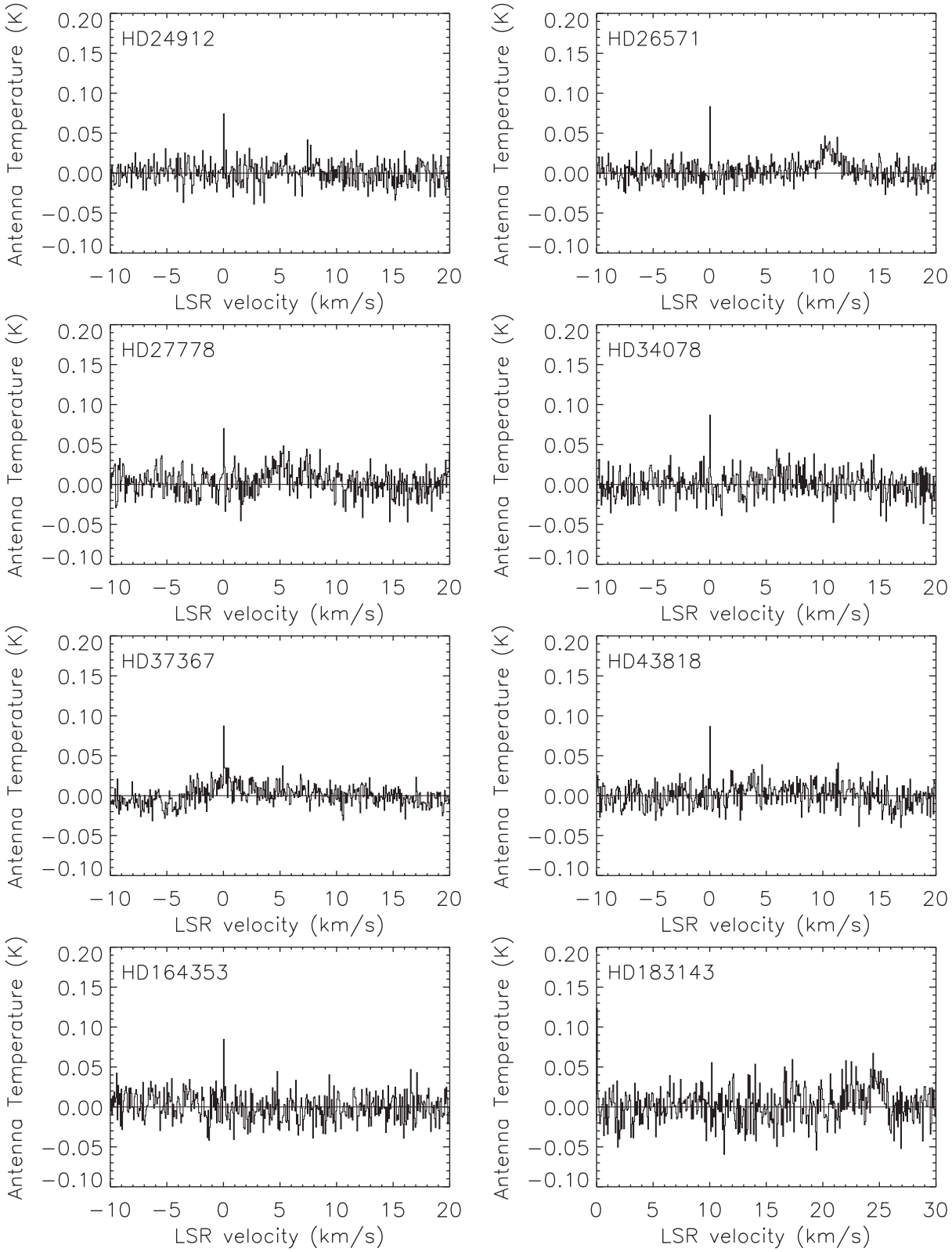

Figure 1(b) – *Continue*.

3 RESULTS

We observed 16 lines of sight towards early-type stars behind or within molecular clouds. The stars are listed in Table 1 along with their coordinates, spectral types, distances to the stars, and distances to the cloud in the line of sight to the star (if known). We detected the 3335-MHz main line for nine lines of sight. In Table 2, we list the Gaussian-fit parameters (antenna temperature, T_A; FWHM, Δv; and v_{LSR}) for all CH detections including 1σ uncertainties. Non-detections are listed as 2σ upper limits in T_A.

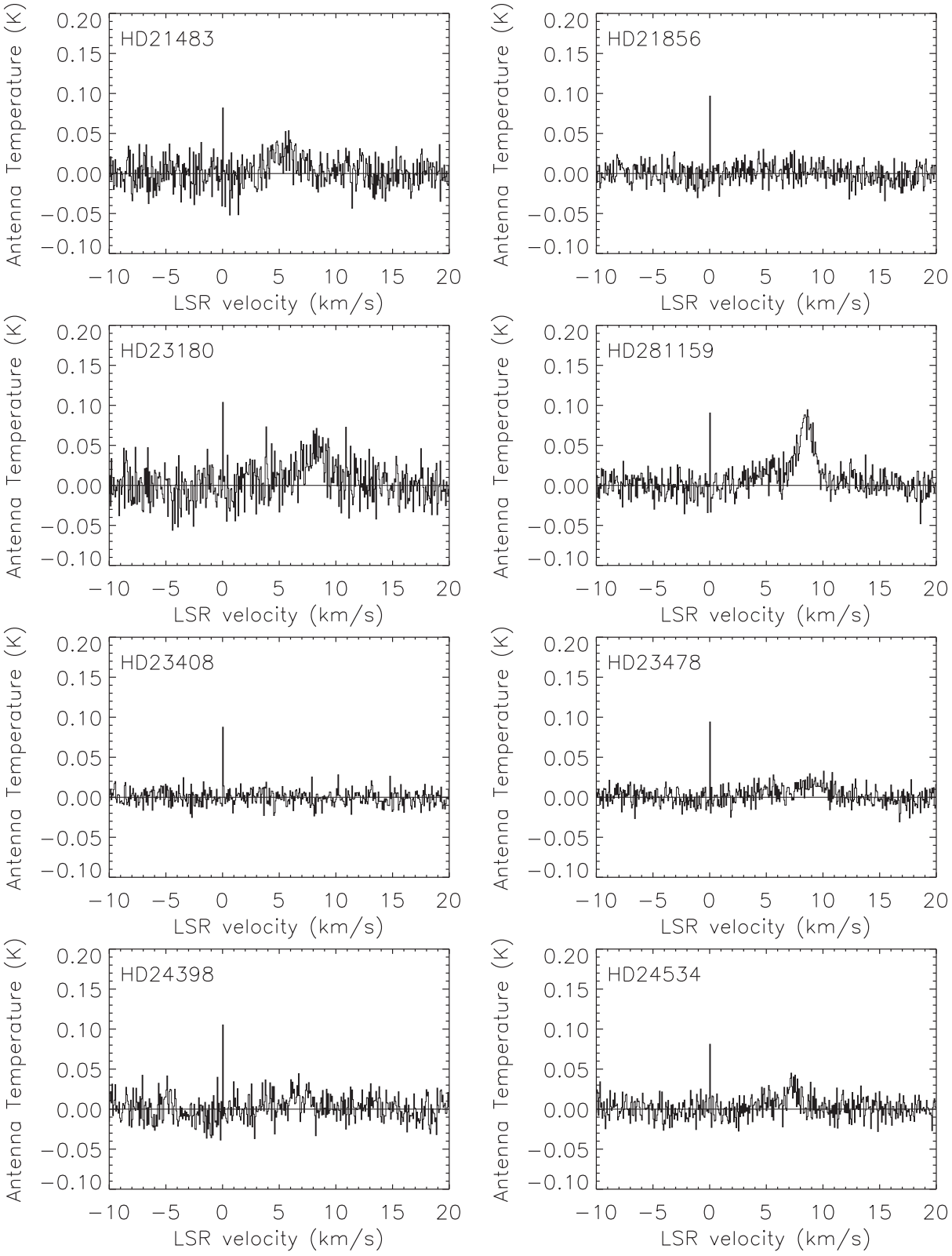

Figure 1(c) – *Continue*.

Table 3 lists the colour excess, $E(B-V)$, for the entire line of sight from Schlafly & Finkbeiner (2011) in column 2. The colour excess along the line of sight to the star is listed in column 3, and is determined from the B and V colours of the star from Oja (1991, 1993), Høg et al. (2000), and Ducati (2002), and the unreddened $B-V$ for the spectral type of the star listed in table 1 from Fitzgerald (1970). Column 4 has W(CH) for the 3335-MHz line as derived by summing the antenna temperature per channel over the line profile.

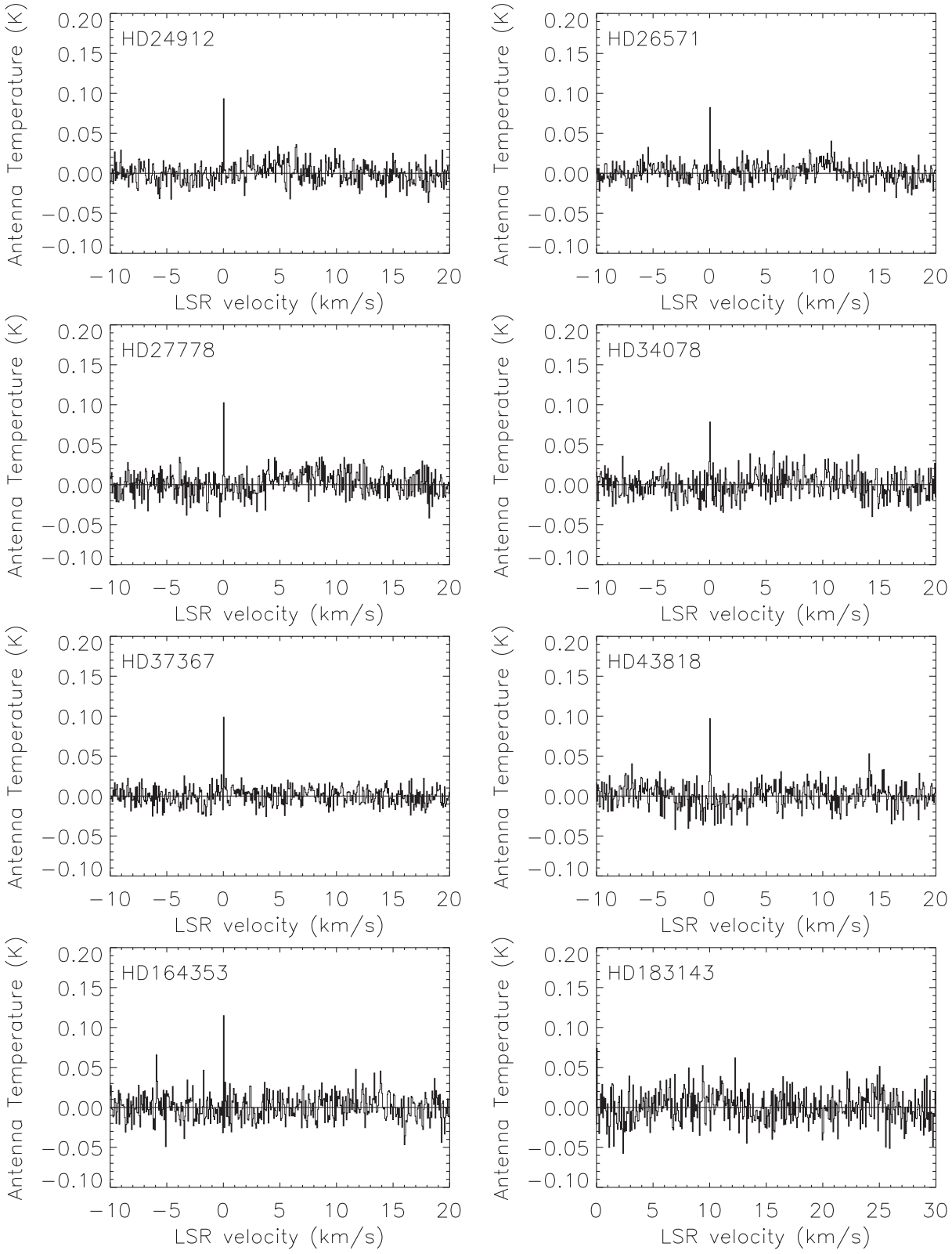

Figure 1(d) – *Continue*.

The uncertainty in W(CH) is calculated using

$$\sigma_{\rm I} = \sqrt{N}\sigma_{\rm T}\Delta v_{\rm c}, \quad (2)$$

where $\sigma_{\rm T}$ is the uncertainty in the antenna temperature, N is the number of channels the line extends over, and $\Delta v_{\rm c}$ is the width of each channel (e.g. Mangum & Shirley 2015). Column 5 lists N(CH) derived from equation (1), and columns 6

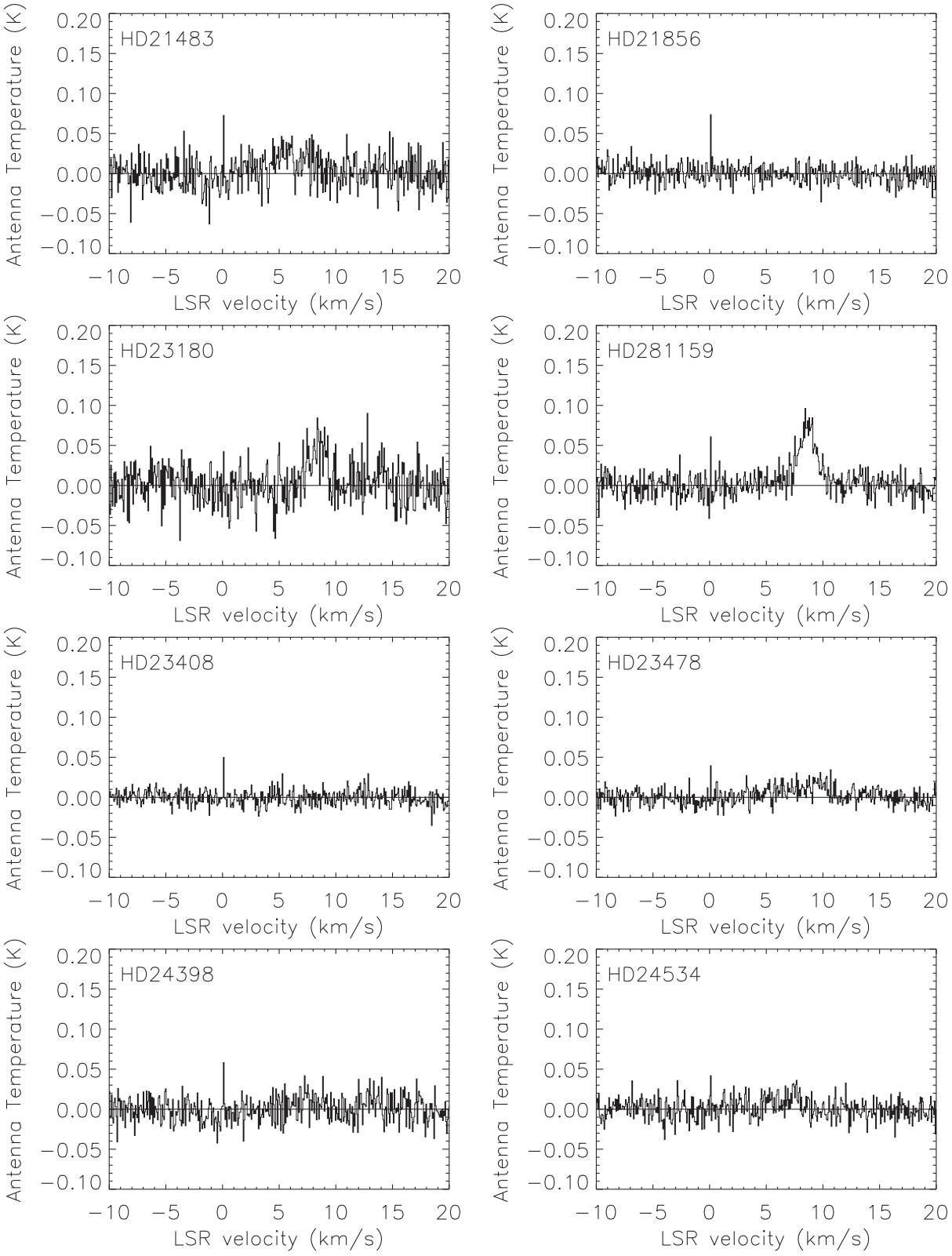

Figure 1(e) – *Continue*.

and 7 list the values of T_{ex} and its uncertainties. For lines of sight with no radio detection, the range of T_{ex} is calculated for the range of values below the 2σ upper limit of the velocity-integrated antenna temperature. As shown in Fig. 2, in cases where W(CH) is fairly large but the corresponding optically determined N(CH) is small, the range of T_{ex} can be well constrained.

We list in Table 4 the velocity-integrated brightness temperatures from the literature in column 2 compared to our observations in column 4 and, in column 5, N(CH) from our data assuming $T_{ex}/(T_{ex}$

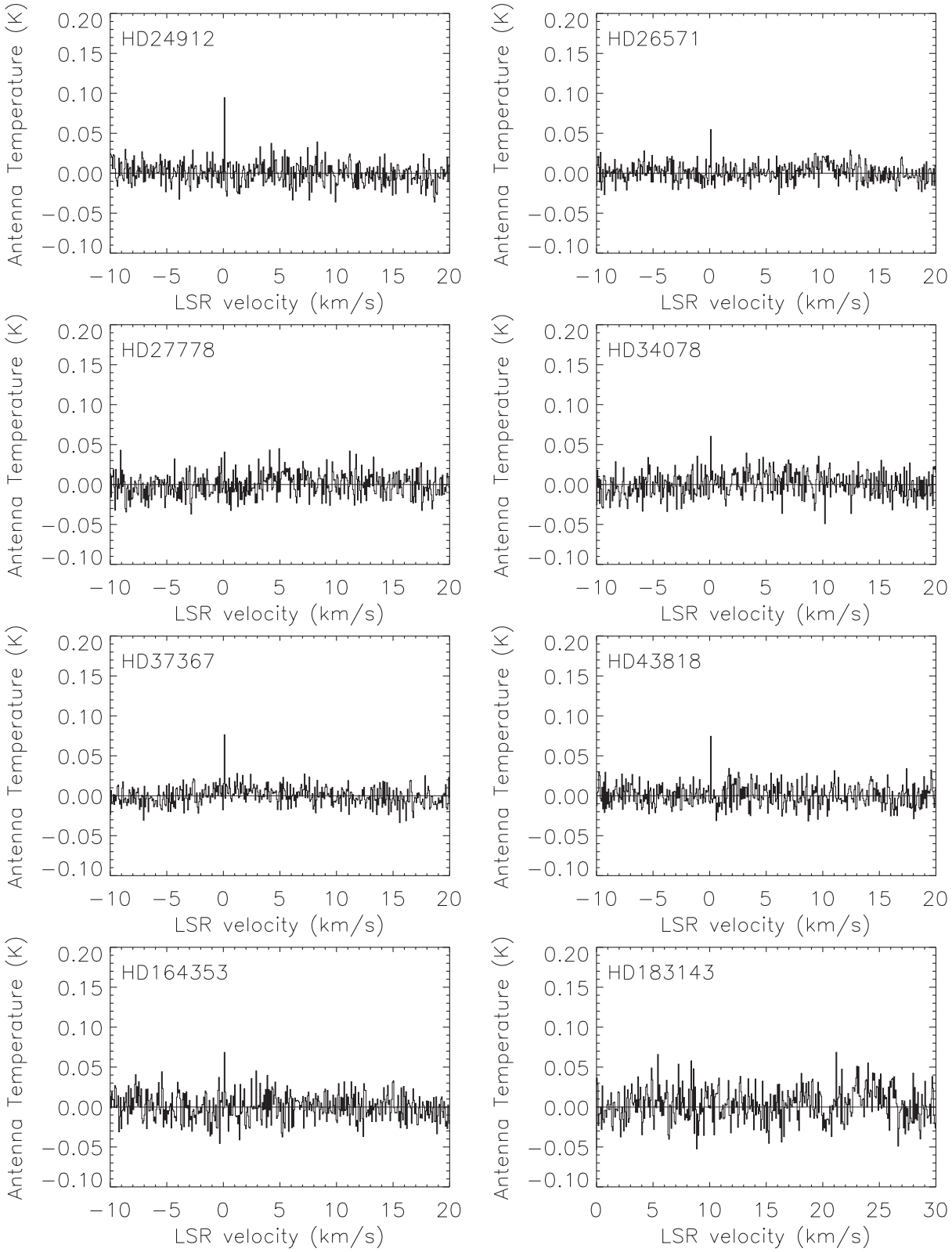

Figure 1(f) – *Continue*.

$- T_{bg}) = 1$. Column 6 lists the value of N(CH) as determined from optical observations in the literature.

Using the technique described in Section 1, we determine T_{ex} for the nine lines of sight where we have values of $W(CH)_{radio}$. The uncertainties for the excitation temperature are determined in two ways: First, formal uncertainties using standard error propagation analysis are listed in column 6 of Table 3. For the second method, assuming $\eta_f = 1$, we can express T_{ex} as

$$T_{ex} = T_{bg}[D/(D-1)] \quad (3)$$

Table 1. Target stars data and distances.

HD number	Name	Spectral type	R.A. (2000) ($^h\ ^m\ ^s$)	Dec. (2000) ($^\circ\ '\ ''$)	ℓ (deg)	b (deg)	d_{star} (pc)	d_{cloud} (pc)
HD 21483	–	B3III[a]	03 28 46.7	+30 22 31.2	158.9	− 21.3	533 ± 32[b]	284^{+8c}_{-5}
HD 21856	–	B1V[a]	03 32 40.0	+35 27 42.2	156.3	− 16.8	465 ± 24[b]	–
HD 23180	*o* Per	B1III[d]	03 44 19.1	+32 17 17.7	160.4	− 17.7	344 ± 86[e]	321 ± 10[f]
HD 281159	–	B5V[g]	03 44 34.2	+32 09 46.3	160.5	− 17.8	152 ± 94[e]	321 ± 10[f,h]
HD 23408	20 Tau	B7III[i]	03 45 49.6	+24 22 03.9	166.2	− 23.5	118 ± 4[e]	–
HD 23478	–	B3IV[j]	03 46 40.9	+32 17 24.7	160.8	− 17.4	288 ± 5[b]	299^{+10c}_{-8}
HD 24398	ζ Per	B1Ib[k]	03 54 07.9	+31 53 01.1	162.3	− 16.7	230 ± 10[e]	140–170[l,m]
HD 24534	X Per	O9.5III[n]	03 55 23.1	+31 02 45.0	163.1	− 17.1	810 ± 37[b]	140–170[l,m]
HD 24912	ξ Per	O7.5III(n)((f))[o]	03 58 57.9	+35 47 27.7	160.4	− 13.1	382 ± 74[e]	–
HD 26571	V1137 Tau	B8III[p]	04 12 51.2	+22 24 48.5	172.4	− 20.6	274 ± 8[b]	140 ± 10[l]
HD 27778	62 Tau	B3V[i]	04 23 59.8	+24 18 03.5	172.8	− 17.4	224 ± 2[b]	140 ± 10[l]
HD 34078	AE Aur	O9.5V[o]	05 16 18.1	+34 18 44.3	172.1	− 02.3	406 ± 11[b]	–
HD 37367	–	B2IV-V[k]	05 39 18.3	+29 12 54.8	179.0	− 01.0	989 ± 167[b]	–
HD 43818	11 Gem	B0II[a]	06 19 19.3	+23 28 09.9	188.5	+03.9	2570 ± 300[b]	–
HD 164353	67 Oph	B5I[q]	18 00 38.7	+02 55 53.6	029.7	+12.6	566 ± 159[b]	–
HD 183143	–	B6Ia[r]	19 27 26.6	+18 17 45.2	053.2	+00.6	2440 ± 270[e]	–

Note. (a) Wenger et al. (2000). (b) Distance based on parallax from Gaia Collaboration (2016, 2018). (c) Zucker et al. (2019). (d) Morgan & Keenan (1973). (e) Distance based on parallax from the *Hipparcos* Catalogue (van Leeuwen 2007). (f) Ortiz-León et al. (2018). (g) Mora et al. (2001). (h) distance to the cloud with highest extinction – foreground clouds at 169^{+2}_{-3} pc likely contribute to the absorption in the optical (Zucker et al. 2018). (i) Pesch (1967). (j) Hiltner (1956). (k) Lesh (1968). (l) Kenyon, Dobrzycka & Hartmann (1994). (m) Zucker et al. (2018). (n) Slettebak (1982). (o) Sota et al. (2011). (p) Hube (1970). (q) van Belle & von Braun (2009). (r) Stock, Nassau & Stephenson (1960).

where D is

$$D = N(\mathrm{CH})[W(\mathrm{CH}) \times (2.82 \times 10^{11})]^{-1}. \quad (4)$$

For values of D approaching 1, the value of T_{ex} becomes singular. Thus a calculation of the uncertainties based on error propagation becomes indeterminate. For those lines of sight where $N(\mathrm{CH})_{optical}$ and $W(\mathrm{CH})_{radio}$ lead to values of D approaching 1, we can determine the range of T_{ex} based on $D \pm 1\sigma$.

3.1 Comparison with previous observations

We compare our values of the velocity integrated brightness temperature, W(CH), obtained with a ∼1.4 arcmin beam to the data presented by Lang & Willson (1978) and Willson (1981) with a ∼9 arcmin beam (see Table 4). Due to the large discrepancy in beam sizes, inconsistencies with the results of Lang & Willson (1978) and Willson (1981) are likely attributable to structure in the two beams and underscore the importance of minimizing the radio beam when comparing the radio and optical observations. Twelve of sixteen of our lines of sight were observed by Liszt (2008) for the ^{12}CO J = 1–0 line at 115.3 GHz using the ARO 12-m telescope, with a beam size of 65 arcsec. He detected CO emission from 7 of 12 lines of sight included in Table 1, with each detection/non-detection mirrored by our CH results in Table 2.

4 PROBLEMS IN DETERMINING T_{EX}

The excitation temperature is derived by the method described in the introduction but several concerns must be addressed. We assume that η_f is 1.0; should there be significant structure on the scale of 10^{-2} pc, then optical and radio comparisons would be unprofitable.

For three of the nine lines of sight with radio detections, the 1σ uncertainty from the measurements of the optical and radio CH lines extends over the singularity in equation (3). Lien (1984) first pointed out this issue in his calculations of the excitation temperature. The excitation temperature rapidly increases in both positive and negative value as it approaches this singularity. Consequently, accurate measurements are required in order to calculate T_{ex} accurately. For the remaining six lines of sight, the range of optical and radio 1σ uncertainty does not result in an excitation temperature that approaches the singularity, and the values of T_{ex} are between −3.1 K $< T_{ex} <$ 10 K.

We primarily used parallax measurements and cloud distance measurements from literature shown in Table 1 to determine the position of the star relative to the cloud. Secondarily, we used colour excess of the line of sight to the star compared with the colour excess of the full line of sight as shown in Table 3 to determine if the optical and radio observations are observing equivalent material. For five lines of sight, the star is behind the cloud according to the cloud distance determined from Ĉernis (1993), Kenyon et al. (1994), Arce et al. (2011), and Zucker et al. (2018, 2019). In these instances, we can assume that the optical and radio beam are sampling the same molecular column.

The remaining four stars with radio detections are either within or very close to the cloud, or we lack information on the cloud distance and the colour excess is unreliable for the line of sight. The proximity to the cloud means that the CH column detected in the optical may not be equivalent to that detected in radio. In addition, dust extinction is a cumulative quantity, making it hard to attribute the entire value solely to a single molecular cloud in front of the star. Ĉernis (1993) and Zucker et al. (2018) have shown the extinction along a line of sight can occur in discrete increments due to intervening clouds. For example, Ĉernis (1993) discusses two dust layers in the direction of IC348, at 160 ± 20, and 260 ± 20 pc, and with A_V = 0.71 ± 0.27 and 2.0 ± 0.6 mag, respectively.

4.1 Alternate measurements of T_{ex}

In addition to the method described in Section 2, we also use the method described in Lien (1984) to determine the excitation temperatures towards a few of our lines of sight using optical data

Table 2. Radio CH observations.

Line of sight	Integration time (min)	T_A (3335.5) (mK)	Δv (km s^{-1})	v_{LSR} (km s^{-1})	T_A (3349.2) (mK)	Δv (km s^{-1})	v_{LSR} (km s^{-1})	T_A (3263.8) (mK)	Δv (km s^{-1})	v_{LSR} (km s^{-1})
HD 21483	35[a]	45.7 ± 17.2	1.35 ± 0.51	5.69	28.2 ± 17.6	2.60 ± 1.63	5.51	21.5 ± 18.3	4.02 ± 3.41	6.01
HD 21856	90[b]	<22.8	–	–	<22.8	–	–	<22.6	–	–
HD 23180	25[a]	75.7 ± 21.7	1.81 ± 0.52	8.41	37.1 ± 20.8	3.33 ± 1.87	8.19	51.6 ± 22.4	1.63 ± 0.71	8.37
HD 281159	60[b]	115.5 ± 12.6	1.48 ± 0.16	8.66	79.0 ± 12.7	1.74 ± 0.28	8.50	73.9 ± 13.0	1.84 ± 0.32	8.63
		24.0 ± 12.6	5.69 ± 2.99	7.23	17.8 ± 12.7	2.85 ± 2.03	5.14			
HD 23408	120[b]	<18.3	–	–	<17.1	–	–	<18.1	–	–
HD 23478	120[b]	13.9 ± 9.3	1.63 ± 1.10	9.56	14.0 ± 9.4	4.57 ± 3.05	8.74	13.6 ± 9.2	5.20 ± 3.53	8.60
		16.4 ± 9.3	4.81 ± 2.74	8.25						
HD 24398	50[a]	26.0 ± 14.6	1.77 ± 0.99	7.60	16.8 ± 14.5	2.29 ± 1.97	6.72	<30.9	–	–
HD 24534	75[a]	44.8 ± 12.3	0.77 ± 0.21	7.55	22.5 ± 11.6	1.97 ± 1.02	7.24	[21.5 ± 12.4]	[1.21 ± 0.70]	[7.43]
		23.0 ± 12.3	4.88 ± 2.61	6.58						
HD 24912	70[b]	<25.3	–	–	<25.4	–	–	<26.7	–	–
HD 26571	105[b]	28.4 ± 10.2	2.12 ± 0.76	10.50	[14.0 ± 10.2]	[2.24 ± 1.63]	[10.10]	[12.9 ± 10.3]	[2.31 ± 1.84]	[10.09]
HD 27778	50[a]	17.0 ± 14.7	4.73 ± 4.11	5.70	<29.8	–	–	<29.1	–	–
HD 34078	50[b]	<30.8	–	–	<30.9	–	–	<30.2	–	–
HD 37367	90[b]	[20.5 ± 10.9]	[2.91 ± 1.54]	[0.25]	<20.1	–	–	<21.2	–	–
HD 43818	55[b]	<27.7	–	–	<27.2	–	–	<27.4	–	–
HD 164353	45[a]	<32.0	–	–	<32.7	–	–	<31.5	–	–
HD 183143	30[a]	31.2 ± 18.9	1.39 ± 0.84	24.36	<37.4	–	–	<41.7	–	–

Notes. Brackets indicate a tentative detection. Spectra for each line of sight are shown in Fig. 1.
(a) $\eta_B = 0.57 \pm 0.02$ – see Section 2.
(b) $\eta_B = 0.40 \pm 0.04$ – see Section 2.

from Jura & Meyer (1985), Weselak et al. (2008, 2014), and Weselak (2019). The excitation temperature is calculated by using the 3886-Å line to derive the upper column density (N_u) and the 3890-Å line to derive the lower column density (N_l) of the lambda-doubled levels. With values for N_u and N_l, T_{ex} may be determined using an equation from Lien (1984):

$$T_{ex} = 0.16[\ln(N_l/N_u)]^{-1} \quad (5)$$

The uncertainties for the excitation temperature are determined in two ways: First, using formal propagation of error, and secondly using the range of column density $N \pm 1\sigma$ for the 3886 and 3890 Å lines to find informal limits to the excitation temperature. The results are shown in Table 5 with columns 2 and 3 listing the values for the column density of the upper and lower levels according to various observers (column 4). Column 5 has the ratio of $N(CH)_l$ and $N(CH)_u$. Column 6 has the calculated T_{ex} from equation (3), and column 7 has the range of T_{ex} determined using the $\pm 1\sigma$ range as described above. For the majority of these lines of sight, there is a singularity in the range of excitation temperatures which causes a large range of values of T_{ex}. However, there is some overlap between the ranges of T_{ex} for a given line of sight. For example, the line of sight to ζ Per has the range -1.12 K $> T_{ex} > -2.41$ K in common between the five data sets.

5 DISCUSSION

Rydbeck et al. (1976) found $T_{ex} = -15 \pm 5$ K by making on–off observations of the CH 3335-MHz line towards Cas A. Calculating T_{ex}, using optical observations or a combination of optical and radio observations, consistent with $T_{ex} = -15 \pm 5$ K requires very accurate measurements of N_l/N_u or D. Fig. 3 shows that the rapid change in slope near the singularity (at D or $N_l/N_u = 1$) necessitates increasingly accurate measurements of D or N_l/N_u if a reliable range of T_{ex} is to be derived. For example, the ratio of the lower and upper column densities determined from optical observations in Table 5 has average uncertainties of ± 0.13, for average values of $N_l/N_u \approx 1$. This then limits the range of T_{ex} to 1.3 K $> T_{ex} > -1.1$ K. Reproducing the calculation of T_{ex} as determined by Rydbeck et al. (1976) ($T_{ex} = -15 \pm 5$ K) by the ratio of lower and upper column densities requires $N_l/N_u = 0.9894^{+0.0026}_{-0.0053}$, necessitating highly accurate measurements of N_l/N_u. By using a combination of optical and radio measurements, reproducing the Rydbeck et al. (1976) value would require $D = 0.8427^{+0.0345}_{-0.0614}$.

Hjalmarson et al. (1977) determined $T_{ex} = -9 \pm 4$ K using on–off observations with the Onsala Space Observatory 25.6-m telescope (15 arcmin beam at 3.3 GHz) towards 3C 123 near the dark cloud L1500, consistent with $T_{ex} = -15$ (+10, −30) K determined by Rydbeck et al. (1976). However, we derive $T_{ex} = -3$ K using the line and continuum values given by Hjalmarson et al. (1977) and their equation 3. Liszt & Lucas (2002) determined $T_{ex} = -10.7 \pm 3.2$ K towards 3C 123 using observations with the NRAO 43-m telescope, with a beam size of approximately 9 arcmin, consistent with $T_{ex} = -9 \pm 4$ K from Hjalmarson et al. (1977) despite the varying beam sizes. The values from Liszt and Lucas (2002) and Hjalmarson et al. (1977), whether $T_{ex} = -9$ or -3 K, differ greatly from the value from Genzel et al. (1979) determined using the Effelsberg 100-m telescope (4 arcmin beam at 3.3 GHz) for the same line of sight, $T_{ex} = -60 \pm 30$ K.

We now discuss our results for each of our detections.

Table 3. Column densities and excitation temperatures derived from our data.

Line of sight	$E(B-V)^a_{\rm full}$	$E(B-V)^b_{\rm star}$	$W(\rm CH)^c_{\rm radio}$ (mK km s^{-1})	$N(\rm CH)^d_{\rm radio}$ (10^{12} cm^{-2})	$T^e_{\rm ex}$ (K)	$T^f_{\rm ex}$ (K)
HD 21483	0.89 ± 0.14	0.52	149 ± 19	42.1 ± 5.3	−35 ± 69	$T_{\rm ex} > 48$, $T_{\rm ex} < -11$
HD 21856	0.28 ± 0.04	0.17	<60.7	<17.1	–	$T_{\rm ex} > 2.8$, $T_{\rm ex} < -2.7$
HD 23180	3.49 ± 0.56	0.31	327 ± 31	92.2 ± 8.8	−0.73 ± 0.09	$-0.64 > T_{\rm ex} > -0.82$
HD 281159	8.90 ± 1.42	0.84	801 ± 86	226 ± 24	−0.86 ± 0.15	$-0.72 > T_{\rm ex} > -1.0$
HD 23408	0.59 ± 0.09	0.05	<48.6	<13.7	–	$T_{\rm ex} > 2.8$, $T_{\rm ex} < -0.28$
HD 23478	0.56 ± 0.09	0.24	215 ± 30	60.6 ± 8.4	−1.2 ± 0.3	$-1.0 > T_{\rm ex} > -1.5$
HD 24398	0.27 ± 0.04	0.31	76.5 ± 15.6	21.6 ± 4.4	−27 ± 58	$T_{\rm ex} > 34$, $T_{\rm ex} < -7.2$
HD 24534	0.38 ± 0.06	0.42	260 ± 20	73.2 ± 5.7	−3.1 ± 0.5	$-2.6 > T_{\rm ex} > -3.7$
HD 24912	0.26 ± 0.04	0.33[g]	<67.4	<19.0	–	$T_{\rm ex} > 2.8$, $T_{\rm ex} < -11$
HD 26571	0.41 ± 0.07	0.29	182 ± 27	51.4 ± 7.5	−1.8 ± 0.7	$-1.2 > T_{\rm ex} > -2.6$
HD 27778	0.53 ± 0.09	0.36	135 ± 24	38.0 ± 6.6	−55 ± 197	$T_{\rm ex} > 27$, $T_{\rm ex} < -10$
HD 34078	1.95 ± 0.31[h]	0.52	<82.0	<23.1	–	$5.7 > T_{\rm ex} > 2.8$
HD 37367	1.32 ± 0.21[h]	0.37	<58.1	<16.4	–	$T_{\rm ex} > 2.8$, $T_{\rm ex} < -40$
HD 43818	0.97 ± 0.16[h]	0.58	<73.7	<20.8	–	$T_{\rm ex} > 2.8$, $T_{\rm ex} < -4.2$
HD 164353	0.18 ± 0.03	0.12	<59.9	<16.9	–	$T_{\rm ex} > 2.8$, $T_{\rm ex} < -1.0$
HD 183143	3.40 ± 0.54[h]	1.29	129 ± 31	36.4 ± 8.8	10 ± 7	$89 > T_{\rm ex} > 6.7$

Notes. (a) Calculated using A_V from the NED Extinction Calculator using data from Schlafly & Finkbeiner (2011) with $E(B-V) = A_V/3.1$.
(b) Calculated by method described in Section 3.
(c) W(CH) determined with a non-parametric fit of the data. 2σ upper limits of W(CH) calculated using $\rm W(CH) = 1.066(T_A \Delta v)/(\eta_B)$ assume $\Delta v = 1$ km s^{-1}.
(d) $N(\rm CH)_{\rm radio}$ assuming that $T_{\rm ex} \gg T_{\rm bg}$.
(e) Uncertainties based on formal error propagation.
(f) Uncertainties based on the $\pm 1\sigma$ range in D as described in Section 3.
(g) Thorburn et al. (2003).
(h) Unreliable colour excess, $|b| < 5°$ (Schlegel, Finkbeiner & Davis 1998).

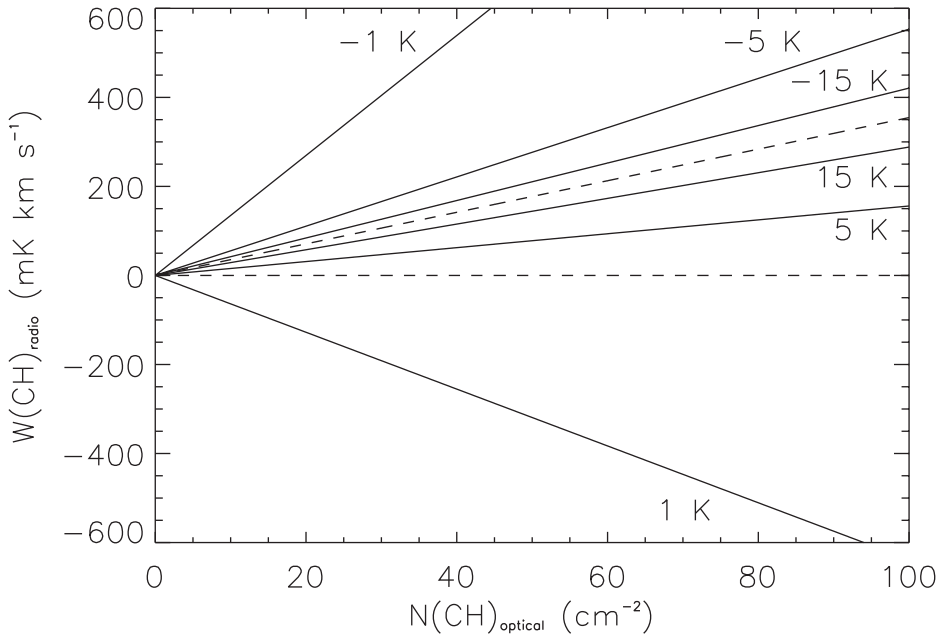

Figure 2. Plot of $W(\rm CH)_{\rm radio}$ as a function of $N(\rm CH)_{\rm optical}$ ($\times 10^{12}$) for various $T_{\rm ex}$. The upper dotted line is for large $T_{\rm ex}$, when $T_{\rm ex}/(T_{\rm ex} - T_{\rm bg}) = 1$. The lower dotted line at $T_{\rm ex} = 2.8$ K shows the transition from emission to absorption, at which there is no detectable radio signal and $T_{\rm ex}/(T_{\rm ex} - T_{\rm bg})$ is undefined. The plot assumes $\eta_{\rm f} = 1$ and $T_{\rm bg} = 2.8$ K. See discussion in Section 3.

5.1 HD 21483

The parallax data from SIMBAD give a distance of 533 ± 32 pc for HD 21483, placing it behind an intervening portion of the Perseus clouds at 284^{+8}_{-5} pc (Zucker et al. 2019). The colour excesses to the star and along the line of sight are 0.52 and 0.89 ± 0.14 mag, respectively, which along with the cloud and star distances suggests that the radio and optical beams are sampling approximately the same molecular material. Using the optical column density from Thorburn et al. (2003), we find $T_{\rm ex} = -35 \pm 69$ K. However, the 1σ uncertainty in D encompasses the singularity, resulting in a large range of $T_{\rm ex}$ (from the 1σ uncertainty in D) with $T_{\rm ex} > 48$ K, $T_{\rm ex} < -11$ K.

Table 4. Data from literature.

Position	$W(CH)^{a}_{radio}$ Literature (mK km s^{-1})	Ref	$W(CH)^{b}_{radio}$ This paper (mK km s^{-1})	$N(CH)^{c}_{radio}$ This paper (10^{12} cm^{-2})	$N(CH)_{optical}$ Literature (10^{12} cm^{-2})	Ref
HD 21483	203 ± 44	*d*	149 ± 19	42.1 ± 5.3	39 ± 3	*e*
HD 21856	–		<60.7	<17.1	6.90 ± 0.76	*f*
HD 23180	286 ± 47	*d*	327 ± 31	92.2 ± 8.8	19.00 ± 0.22	*g*
HD 281159	391 ± 32	*h*	801 ± 86	226 ± 24	53 ± 4	*e*
HD 23408	<71.1	*h*	<48.6	<13.7	1.5 ± 0.6	*i*
HD 23478	–		215 ± 30	60.6 ± 8.4	18.3 ± 0.7	*j*
HD 24398	139 ± 14	*h*	76.5 ± 15.6	21.6 ± 4.4	19.52 ± 0.24	*g*
HD 24534	134 ± 14	*h*	260 ± 20	73.2 ± 5.7	38.49 ± 0.60	*k*
HD 24912	<88.8	*h*	<67.4	<19.0	11.99 ± 0.34	*g*
HD 26571	84.4 ± 21.6	*h*	182 ± 27	51.4 ± 7.5	20 ± 4	*e*
HD 27778	–		135 ± 24	38.0 ± 6.6	36.14 ± 0.36	*k*
HD 34078	<107	*h*	<82.0	<23.1	70.80 ± 0.44	*g*
HD 37367	–		<58.1	<16.4	12.0 ± 2.4	*l*
HD 43818	–		<73.7	<20.8	11.3 ± 2.2	*l*
HD 164353	–		<59.9	<16.9	4.4 ± 2.2	*i*
HD 183143	–		129 ± 31	36.4 ± 8.8	50 ± 3	*e*

Notes. (a) $W(CH)_{radio}$ calculated using η_B, T_A, and Δv, from references in column 3. $W(CH) = 1.066(T_A \Delta v)/(\eta_B)$. For 2σ upper limits, Δv is assumed to be 1 km s^{-1}.
(b) Same as column 4 of Table 3.
(c) Radio column densities assume $T_{ex} \gg T_{bg}$.
(d) Lang & Willson (1978).
(e) Thorburn et al. (2003).
(f) Weselak (2019).
(g) Weselak et al. (2014).
(h) Willson (1981).
(i) Federman (1982).
(j) Sheffer & Federman (2007).
(k) Weselak et al. (2008).
(l) Sheffer et al. (2008).

Table 5. T_{ex} from optical measurements from the literature.

Position	N_u (3886) (10^{12} cm^{-2})	N_l (3890) (10^{12} cm^{-2})	Ref	N_l/N_u	T^{a}_{ex} (K)	T_{ex} range^{b} (K)
HD 23180	8.91 ± 0.24	9.30 ± 0.32	*c*	1.04 ± 0.05	3.73 ± 3.81	$T_{ex} > 1.54$, $-8.53 > T_{ex}$
	9.82 ± 0.70	12.97 ± 0.70	*d*	1.32 ± 0.12	0.57 ± 0.19	$1.04 > T_{ex} > 0.39$
	9.89 ± 0.70	10.62 ± 0.91	*e*	1.07 ± 0.12	2.25 ± 3.51	$T_{ex} > 0.71$, $-1.84 > T_{ex}$
	10.54 ± 1.29	11.46 ± 1.51	*f*	1.09 ± 0.19	1.91 ± 4.11	$T_{ex} > 0.47$, $-0.93 > T_{ex}$
HD 24398	20.5 ± 0.4	18.1 ± 0.5	*c*	0.88 ± 0.03	−1.29 ± 0.32	$-0.96 > T_{ex} > -1.96$
	10.05 ± 0.47	9.82 ± 0.70	*d*	0.98 ± 0.08	−6.69 ± 23.8	$T_{ex} > 1.73$, $-1.12 > T_{ex}$
	11.54 ± 0.84	11.04 ± 0.95	*e*	0.96 ± 0.11	−3.61 ± 9.19	$T_{ex} > 1.41$, $-0.78 > T_{ex}$
	11.60 ± 1.17	10.55 ± 1.33	*f*	0.91 ± 0.15	−1.69 ± 2.90	$T_{ex} > 1.22$, $-0.49 > T_{ex}$
HD 24534	18.94 ± 1.87	19.28 ± 1.05	*d*	1.02 ± 0.11	8.91 ± 56.0	$T_{ex} > 0.91$, $-1.21 > T_{ex}$
	19.85 ± 2.36	19.46 ± 1.51	*f*	0.98 ± 0.14	−7.99 ± 56.7	$T_{ex} > 0.88$, $-0.75 > T_{ex}$
HD 24912	6.73 ± 0.94	6.76 ± 0.98	*e*	1.00 ± 0.20	36.0 ± 1630	$T_{ex} > 0.55$, $-0.57 > T_{ex}$
	7.20 ± 1.31	8.59 ± 1.58	*f*	1.19 ± 0.31	0.91 ± 1.33	$T_{ex} > 0.29$, $-0.83 > T_{ex}$
HD 27778	18.00 ± 2.10	17.88 ± 2.10	*d*	0.99 ± 0.16	−23.2 ± 556	$T_{ex} > 0.70$, $-0.66 > T_{ex}$
	16.90 ± 2.06	16.20 ± 2.8	*e*	0.96 ± 0.20	−3.78 ± 18.9	$T_{ex} > 0.65$, $-0.46 > T_{ex}$
	22.79 ± 1.82	16.90 ± 2.24	*f*	0.74 ± 0.11	−0.53 ± 0.28	$-0.31 > T_{ex} > -1.75$
HD 34078	37.87 ± 0.70	37.16 ± 0.70	*d*	0.98 ± 0.03	−8.38 ± 11.6	$T_{ex} > 8.74$, $-2.83 > T_{ex}$
	45.80 ± 2.58	41.90 ± 3.58	*e*	0.91 ± 0.09	−1.80 ± 2.07	$T_{ex} > 2.79$, $-0.71 > T_{ex}$
	39.16 ± 3.06	39.54 ± 1.75	*f*	1.01 ± 0.09	16.5 ± 152.8	$T_{ex} > 1.19$, $-1.44 > T_{ex}$

Notes. (a) Uncertainties based on formal error propagation.
(b) Uncertainties based on technique we described in Section 4.1.
(c) Jura & Meyer (1985).
(d) Weselak et al. (2008).
(e) Weselak et al. (2014).
(f) Weselak (2019).

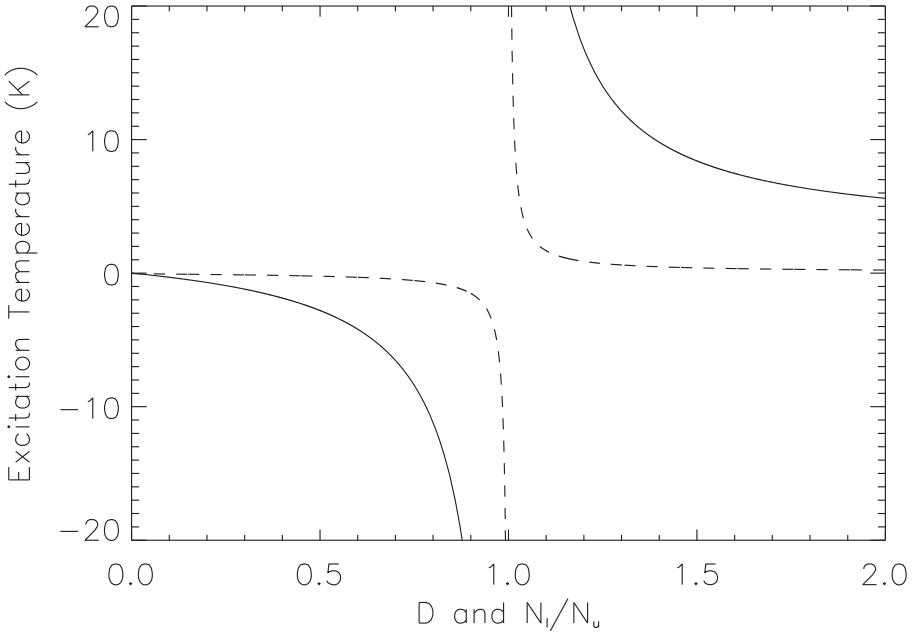

Figure 3. Plot of T_{ex} as a function of the ratio of the population in the lower and upper levels of the lambda-doubled CH ground state (dashed lines) and the function $D = N(\mathrm{CH})(\eta_f)[W(\mathrm{CH}) \times (2.82 \times 10^{11})]^{-1}$ (solid lines). See discussion in Section 5.

5.2 HD 23180 (*o* Persei)

The parallax data from SIMBAD give a distance of 344 ± 86 pc for HD 23180, which places it close to the IC348 region at 321 ± 10 pc (Ortiz-León et al. 2018). However, Arce et al. (2011) state that HD 23180 is likely within ∼1 pc of the cluster. The colour excess of the star and along the line of sight are 0.31 and 3.49 ± 0.56 mag, respectively, which along with the cloud and star distances likely indicate that a considerable portion of the molecular gas extends beyond the star. Due to the star's proximity to the cloud, it is likely that the radio observations are sampling CH behind the star which cannot be seen by the optical observations. Using the optical column density from Weselak et al. (2014), we find $T_{ex} = -0.73 \pm 0.09$ K.

This star has been studied by Jura & Meyer (1985) who find the excitation temperature using optical observations of the CH *B*–*X* lines. They find $T_{ex} = 3.7$ K, but the uncertainty of the upper and lower column densities encompasses the singularity in equation (3). The range of values for T_{ex} are inconsistent with the excitation temperature we find, likely due to the component of the cloud behind the star.

5.3 HD 281159

The parallax data for HD 281159 from SIMBAD give a distance of 152 ± 94 pc, likely placing it in front of an intervening portion of the IC348 region at 321 ± 10 pc (Ortiz-León et al. 2018). The small parallax distance likely means the absorption measured in the optical is from the foreground clouds at 169 $^{+2}_{-3}$ pc (Zucker et al. 2018). The colour excess of the star and along the line of sight are 0.84 and 8.90 ± 1.42 mag, respectively, which along with the cloud and star distances likely indicate that the radio velocity-integrated brightness temperature is sampling more of the cloud than the optical measurement. Our $W(\mathrm{CH})_{\mathrm{radio}}$ value does not agree within 4σ with the velocity-integrated brightness temperature from Willson (1981), likely indicating that the CH distribution has structure at scales of a few arcminutes. Using the optical column density from Thorburn et al. (2003), we find $T_{ex} = -0.86 \pm 0.15$ K. Due to the stars proximity to the cloud, it is likely that the radio observations are sampling CH behind the star which is not seen by the optical observations.

5.4 HD 23478

The parallax distance for HD 23478 is 288 ± 5 pc, placing it at about the same distance as an intervening portion of the Perseus clouds at 299$^{+10}_{-8}$ pc (Zucker et al. 2019). The colour excess of the star and along the line of sight are 0.24 and 0.56 ± 0.09 mag respectively, which along with the cloud and star distances could possibly indicate that the radio estimate is sampling more of the cloud than the optical. Using the optical column density from Sheffer & Federman (2007), we find $T_{ex} = -1.2 \pm 0.3$ K.

5.5 HD 24398 (ζ Persei)

The parallax distance for HD 24398 is 230 ± 10 pc, placing it behind an intervening portion of the Taurus clouds at 140–170 pc (Kenyon et al. 1994; Zucker et al. 2018). The colour excesses of the star and along the line of sight are 0.31 and 0.27 ± 0.04 mag, respectively, which suggests that the radio and optical beams are sampling approximately the same molecular gas. Using the optical column density from Weselak et al. (2014), we find $T_{ex} = -27 \pm 58$ K.

The line of sight to this star has been studied before in order to determine the excitation of the CH main line. Lien (1984) determined T_{ex} from the optical column densities of the upper and lower populations of the lambda-doubled ground state, and also through a comparison of the optical and radio measurements. By using the upper and lower populations of the Λ doublet of the B–X system, he determined $T_{ex} = -0.54 \pm 0.30$ K, with a range of $-2.3 < T_{ex} < -0.3$ K, which does not agree with our T_{ex} estimate. Lien also found $T_{ex} = -3.7$ K through a comparison of the optical and radio measurements using a method similar to the one described in

Section 2, which is outside our range of T_{ex}. Jura & Meyer (1985) determined T_{ex} from the optical column densities of the upper and lower populations obtaining $T_{ex} = -1.3$ K, and Liszt & Lucas (2002) similarly determined $T_{ex} \approx -3$ K.

All but one of the above estimates for T_{ex} are between approximately -4 and -1 K. Our result for the range of T_{ex}, where $T_{ex} > 34$ K and $T_{ex} < -7.2$ K is not consistent with other determinations at the 1σ level. However, given all of the above estimates, the often used assumptions, $T_{ex} = -15 \pm 5$ K, $T_{ex} = -60 \pm 30$ K, and $|T_{ex}| \gg T_{bg}$ may not be valid for this line of sight.

5.6 HD 24534 (X Persei)

The parallax data from SIMBAD gives a distance of 810 ± 37 pc, placing it behind an intervening portion of the Taurus clouds at 140–170 pc (Kenyon et al. 1994; Zucker et al. 2018). The colour excesses to the star and along the line of sight are 0.42 and 0.38 ± 0.06 mag, respectively, which along with the cloud and star distances suggests that the radio and optical beams are sampling approximately the same molecular material. Using the optical column density from Weselak et al. (2008), we find $T_{ex} = -3.1 \pm 0.5$ K. Due to the star being far behind the cloud, and no discontinuity in the uncertainty, we find that the assumption $|T_{ex}| \gg T_{bg}$ is clearly invalid for this line of sight.

This star has been studied before in order to determine the excitation of the CH main line. Lien (1984) determined T_{ex} from the optical column densities of the upper and lower populations, and also through a comparison of the optical and radio measurements. By using the upper and lower populations of the Λ doublet, he determined $T_{ex} = -0.63 \pm 0.73$ K, with a range of $T_{ex} > 0.5$ K, $T_{ex} < -0.2$ K, which is consistent with our T_{ex} estimate. He also found $T_{ex} = 7.6$ K through a comparison of the optical and radio measurements, which is outside our range of T_{ex}. However, his radio measurements were made with a beam size of 9 arcmin, which is the likely reason for the discrepancy between our results.

5.7 HD 26571

The parallax data from SIMBAD gives a distance of 274 ± 8 pc for HD 26571, likely placing it behind the Taurus clouds at 140 ± 10 pc (Kenyon et al. 1994). The colour excesses to the star and along the line of sight are 0.29 and 0.41 ± 0.07 mag, respectively, which along with the cloud and star distances suggests that the radio and optical beams are possibly sampling approximately the same molecular material. Using the optical column density from Thorburn et al. (2003), we find $T_{ex} = -1.8 \pm 0.7$ K. Due to the star being behind the cloud, and the data not causing a discontinuity in the uncertainty, our T_{ex} estimate is robust. We find that the often used assumptions, $T_{ex} = -15 \pm 5$ K, $T_{ex} = -60 \pm 30$ K, and $|T_{ex}| \gg T_{bg}$, are clearly invalid for this line of sight.

5.8 HD 27778

The parallax data from SIMBAD gives a distance of 224 ± 2 pc for HD 27778, likely placing it behind the Taurus clouds at 140 ± 10 pc (Kenyon et al. 1994). The colour excesses to the star and along the line of sight are 0.36 and 0.53 ± 0.08 mag, respectively, which along with the cloud and star distances suggests that the radio and optical beams are possibly sampling approximately the same amount of molecular material. Using the optical column density from Weselak et al. (2008), we find $T_{ex} = -55$ K. However, the 1σ uncertainty in D encompasses the singularity, resulting in a large range of T_{ex} (from the 1σ uncertainty in D) $T_{ex} > 27$ K, $T_{ex} < -10$ K.

5.9 HD 183143

While HD 183143 is at 2435 ± 269 pc, there are no estimates of the intervening cloud's distance. However the colour excess values imply that a translucent cloud is intervening. The colour excess of the star and along the line of sight are 1.29 and 3.40 ± 0.54 mag, respectively, which could possibly indicate that the radio velocity-integrated brightness temperature is sampling more of the cloud than the optical measurement. Unfortunately, the star is at $|b| < 5°$, so the colour excess along the line of sight is unreliable (Schlegel et al. 1998). Using the optical column density from Thorburn et al. (2003), we find $T_{ex} = 10 \pm 7$ K.

6 SUMMARY

Observations of the CH 3335-MHz line have been used since 1976 to determine $N(H_2)$ directly from W(CH) usually by assuming $T_{ex} = -15 \pm 5$ K from Rydbeck et al. (1976), $T_{ex} = -60 \pm 30$ K from Genzel et al. (1979), or $|T_{ex}| \gg T_{bg}$ (e.g. Magnani, Sandell & Lada 1992). Lien (1984) explored other ways of determining T_{ex} from optical and radio data and obtained values inconsistent with $|T_{ex}| \gg T_{bg}$. We observed 16 lines of sight in the CH 3335-MHz line, and detected emission from 9 of them. By combining our radio results with optically derived values for N(CH), we solved for the excitation temperature of the transition, T_{ex}. Unfortunately, this method for determining T_{ex} is often problematic because of the differences in how the column density of CH is calculated from optical and radio observations. Primarily, the molecular material sampled by optical observations only extends to the star, requiring the star to be behind the cloud in order for the molecular material sampled in optical and radio to be approximately equivalent. In addition, the differences in the angular sizes of the two sampled regions could cause problems if the CH is not smoothly distributed.

Our results described in Section 5 imply T_{ex} varies significantly over the nine lines of sight. For a line of sight such as HD 21483 where the 1σ uncertainty in D (see Section 3) encompasses the singularity in equation (3), $|T_{ex}|$ is possibly much greater than T_{bg}. However, for other lines of sight where the 1σ uncertainty in D does not encompasses the singularity, the range of T_{ex} includes values of T_{ex} which are inconsistent with $|T_{ex}| \gg T_{bg}$. We determined $T_{ex} = -1.8 \pm 0.7$ K for the line of sight HD 26571, which is inconsistent with the assumptions $T_{ex} = -15 \pm 5$ K, $T_{ex} = -60 \pm 30$ K, and $|T_{ex}| \gg T_{bg}$. The line of sight to HD 24534, with $T_{ex} = -3.1 \pm 0.5$ K, is also inconsistent.

Assuming $T_{ex} = -15 \pm 5$ K, $T_{ex} = -60 \pm 30$ K, or $|T_{ex}| \gg T_{bg}$ for all lines of sight can lead to overestimates or underestimates of the column density. For example, for HD 26571, with $T_{ex} = -1.8 \pm 0.7$ K, the column densities calculated assuming $|T_{ex}| \gg T_{bg}$ will cause N(CH) to be overestimated by approximately a factor of 2.6. Similarly, assuming $T_{ex} = -15$ K will cause an overestimation of approximately a factor of 2.2.

Although the CH 3335 MHz transition provides a reliable way to study the kinematics and distribution of low-density molecular gas, the conversion of W(CH) to N(CH) may not be as straightforward as has often been assumed. Converting the observations to N(CH) requires accurate measurements of T_{ex}. In the absence of such measurements, the normal assumptions about the value of T_{ex} can lead to significant errors in N(CH). Radio astronomers who use the 3335-MHz line as a surrogate for H_2 should interpret their results

allowing for the possibility that the assumption $|T_{ex}| \gg T_{bg}$ may not hold for some or all of their observations.

ACKNOWLEDGEMENTS

The Arecibo Observatory is operated by SRI International under a cooperative agreement with the National Science Foundation (AST-1100968), and in alliance with Ana G. Méndez-Universidad Metropolitana, and the Universities Space Research Association. This work has made use of data from the European Space Agency (ESA) mission Gaia (https://www.cosmos.esa.int/gaia), processed by the Gaia Data Processing and Analysis Consortium (DPAC, https://www.cosmos.esa.int/web/gaia/dpac/consortium). Funding for the DPAC has been provided by national institutions, in particular the institutions participating in the Gaia Multilateral Agreement. This research has made use of the SIMBAD database, operated at CDS, Strasbourg, France, and the NASA/IPAC Extragalactic Database (NED) which is operated by the Jet Propulsion Laboratory, California Institute of Technology, under contract with the National Aeronautics and Space Administration. W.T. Reach and B-G Andersson acknowledge support from NASA contract NNA17BF53C to the Universities Space Research Association (USRA).

We thank the referee, Harvey Liszt, for comments that rectified an error in the calculation of the uncertainties and greatly improved the presentation. We also would like to thank Steve Shore for helpful discussions and comments on the manuscript.

REFERENCES

Allen R. J., Hogg D. E., Engelke P. D., 2015, AJ, 149, 123
Allen R. J., Ivette Rodríguez M., Black J. H., Booth R. S., 2012, AJ, 143, 97
Andersson B-G, Wannier P. G., 1993, ApJ, 402, 585
Arce H. G., Borkin M. A., Goodman A. A., Pineda J. E., Beaumont C. N., 2011, ApJ, 742, 105
Barriault L., Joncas G., Lockman F. J., Martin P. G., 2010, MNRAS, 407, 2645
Černis K., 1993, Balt. Astron., 2, 214
Chaffee F. H., 1974, ApJ, 189, 427
Chaffee F. H., 1975, ApJ, 199, 379
Cotten D. L., Magnani L., Wennerstrom E. A., Douglas K. A., Onello J. S., 2012, AJ, 144, 163
Danks A. C., Federman S. R., Lambert D. L., 1984, A&A, 130, 62
Donate E., Magnani L., 2017, MNRAS, 472, 3169
Ducati J. R., 2002, VizieR Online Data Catalog, 2237
Dunham T., Jr, Adams W. S., 1937a, Publ. Am. Astr. Soc., 9, 5
Dunham T. Jr, Adams W. S., 1937b, PASP, 49, 26
Federman S. R., 1982, ApJ, 257, 125
Federman S. R., Glassgold A. E., Jenkins E. B., Shaya E. J., 1980, ApJ, 242, 545
Federman S. R., Glassgold A. E., Kwan J., 1979, ApJ, 227, 466
Fitzgerald M. P., 1970, A&A, 4, 234
Fixsen D. J. et al., 2011, ApJ, 734, 5
Gaia Collaboration, 2016, A&A, 595, A1
Gaia Collaboration, 2018, A&A, 616, A1
Genzel R., Downes D., Pauls T., Wilson T. L., Bieging J., 1979, A&A, 73, 253
Grenier I. A., Casandjian J. M., Terrier R., 2005, Science, 307, 1292 (GCT)
Hiltner W. A., 1956, ApJS, 2, 389
Hjalmarson Å. et al., 1977, ApJS, 35, 263
Hube D. P., 1970, Mem. RAS, 72, 233
Høg E. et al., 2000, A&A, 335, L27
Jura M., Meyer D. M., 1985, ApJ, 294, 238
Kenyon S. J., Dobrzycka D., Hartmann L., 1994, AJ, 108, 1872
Lada E. A., Blitz L., 1988, ApJ, 326, 69
Lang K. R., Willson R. F., 1978, ApJ, 224, 125
Lesh J. R., 1968, ApJS, 17, 371
Li D. et al., 2018, ApJS, 235, 1
Lien D. J., 1984, ApJ, 224, 125
Liszt H., Lucas R., 2002, A&A, 391, 693
Liszt H. S., 2008, A&A, 492, 743
Magnani L., Onello J. S., 1993, ApJ, 408, 559
Magnani L., Sandell G., Lada E. A., 1992, A&AS, 93, 509
Mangum J. G., Shirley Y. L., 2015, PASP, 127, 266
Mattila K., 1986, A&A, 160, 157
Mora A. et al., 2001, A&A, 378, 116
Morgan W. W., Keenan P. C., 1973, ARA&A, 11, 29
Oja T., 1991, A&AS, 89, 415
Oja T., 1993, A&AS, 100, 591
Ortiz-León G. N. et al., 2018, ApJ, 865, 73
Pesch P., 1967, ApJ, 148, 781
Rydbeck O. E. H., Kollberg E., Hjalmarson Å., Sume A., Elldér J., Irvine W. M., 1976, ApJS, 31, 333
Sandell G., Stevens M. A., Heiles C., 1987, A&A, 179, 255
Schlafly E. F., Finkbeiner D. P., 2011, ApJ, 737, 103
Schlegel D. J., Finkbeiner D. P., Davis M., 1998, ApJ, 500, 553
Sheffer Y., Federman S. R., 2007, ApJ, 659, 1352
Sheffer Y., Rogers M., Federman S. R., Abel N. P., Gredel R., Lambert D. L., Shaw G., 2008, ApJ, 687, 1075
Slettebak A., 1982, ApJS, 50, 55
Sota A., Maíz Apellániz J., Walborn N. R., Alfaro E. J., Barbá R. H., Morrell N. I., Gamen R. C., Arias J. I., 2011, ApJS, 193, 24
Stock J., Nassau J. J., Stephenson C. B., 1960, Hamburger Sternw., Warner & Swasey Obs., C02, 0
Tang N. et al., 2017, ApJ, 839, 8
Thorburn J. A. et al., 2003, ApJ, 584, 339
Truppe S., Hendricks R. J., Tokunaga S. K., Hinds E. A., Tarbutt M. R., 2014, J. Mol. Spectrosc., 300, 70
van Belle G. T., von Braun K., 2009, ApJ, 694, 1085
van Dishoeck E. F., Black J. H., 1986, ApJS, 62, 109
van Dishoeck E. F., Black J. H., 1988, ApJ, 334, 771
van Dishoeck E. F., Black J. H., 1989, ApJ, 340, 273
van Leeuwen F., 2007, A&A, 474, 653
Wannier P. G., Andersson B.-G., Federman S. R., Lewis B. M., Viala Y. P., Shaya E., 1993, ApJ, 407, 163
Wenger M. et al., 2000, A&AS, 143, 9
Weselak T., 2019, A&A, 625, A55
Weselak T., Galazutdinov G. A., Gnaciński P., Krelowski J., 2014, Acta Astron., 64, 277
Weselak T., Galazutdinov G. A., Musaev F. A., Krelowski J., 2008, A&A, 484, 381
Wiesemeyer H. et al., 2018, A&A, 612, A37
Willson R. F., 1981, ApJ, 247, 116
Xu D., Li D., 2016, ApJ, 833, 90
Xu D., Li D., Yue N., Goldsmith P. F., 2016, ApJ, 819, 22
Zucker C., Schlafly E. F., Speagle J. S., Green G. M., Portillo S. K. N., Finkbeiner D. P., Goodman A. A., 2018, ApJ, 869, 83
Zucker C., Speagle J. S., Schlafly E. F., Green G. M., Finkbeiner D. P., Goodman A. A., Alves J., 2019, ApJ, 125, 20

This paper has been typeset from a TEX/LATEX file prepared by the author.